DYNAMIC MODELING AND ROBUST FORCE-POSITION CONTROL OF A VARIABLE STIFFNESS GRIPPER

Ziqing Yu, Jiaming Fu, Bin Yao, George Chiu, Richard Voyles, and Dongming Gan*, *Member, IEEE*

***Abstract*— Variable Stiffness Grippers (VSGs) represent a groundbreaking advancement in robotic manipulation, embodying the seamless integration of flexibility and rigidity to meet the multifaceted challenges of modern automation. These devices leverage the adaptability of compliant modes for handling a wide range of objects yet can switch to a rigid mode for tasks requiring high strength and precision. The management of variable stiffness poses significant challenges, especially in achieving precise control over the gripper's adaptability to objects of varying compliance. This paper proposes a method to provide a combination of position control and force control of a VSG by exploiting the dynamic model and the different stiffness levels. Our research examines active disturbance rejection control (ADRC) and deterministic robust control (DRC), demonstrating their advantages over PID in managing stiffness variations in robotic grippers. We highlight ADRC and DRC's enhanced robustness and adaptability through a comparative analysis, at different stiffness levels and grasping process. These efforts highlight the importance of sophisticated control systems, in distinguishing between stiff and rigid modes effectively, enabling VSGs to handle objects ranging from fragile.**

I. INTRODUCTION

The rapid expansion of the robotics industry has led to significant advancements in the field of grasping control within robotic grippers, extending their functionalities far beyond traditional roles. This progression is a dual response to the industry's growth and its diversification into various sectors such as logistics, healthcare, agriculture, and nuclear safety [1-2]. The initial focus in grasping control research was primarily on ensuring robust support for diverse objects, with a strong emphasis on safety. Contemporary innovations, however, have expanded these applications to include roles in reliable remote sensing via advanced robotic systems [3]. This evolution reflects the industry's increasing demands and the diverse challenges it faces, underlining the ongoing necessity for advancements in grasping mechanisms. As robotic grippers become more integral in multiple fields, the emphasis on enhancing their precision, safety, and adaptability in control systems is paramount. Compliant robotic hands, known for their adaptability, are particularly adept at handling a variety of objects due to their flexibility, ensuring safety in human interactions and with fragile items [4–8]. Despite their strengths, these grippers encounter challenges in handling power when compared to their more rigid counterparts [9]. In contrast, rigid grippers, with their inflexible nature, can pose challenges in interactions with humans.

VSGs epitomize the integration of rigidity and flexibility, both critical elements for tackling the varied challenges in robotic manipulation. While its compliant mode enhances adaptability, it falls short in handling strength and precision, traits that are inherent in its rigid mode [9–11]. On the other hand, the rigidity mode excels in quick responsiveness and robustness. Bridging these contrasting attributes, the innovative concept of variable stiffness robotic grippers has been introduced [12], offering a spectrum of solutions. Among these solutions are grippers inspired by the scales of pangolins, utilizing toothed pneumatic actuators for stiffness adjustment [13], pneumatic-driven grippers with an exoskeleton and self-locking mechanism for varying stiffness [14], and the use of permanent magnets to control stiffness by changing magnetic force between fingers [15]. Additional methods include employing layer jamming techniques for stiffness control through negative pressure [16], tendon-pulled mechanisms to adjust finger stiffness [17], and the use of Shape Memory Alloys (SMA) [18] or low-melting-point materials [19] for dynamic stiffness transitions. Some designs merge hybrid variable stiffness actuators with traditional single-degree-of-freedom (1-DOF) grippers [20], while others enhance Fin Ray structures by adjusting stiffness through rib rotation within their frames [21]. The array of emerging designs and technologies underscores the continuous evolution and potential of variable stiffness grippers in robotic applications.

The control of varying stiffness represents a significant challenge in managing VSGs, essential for handling a diverse range of objects. To effectively manage a diverse array of objects with varying stiffness requirements, the VSG described in [13] operated without sensors and features a two-finger design that prioritizes safety and adaptability in collision scenarios. This was achieved through the use of repulsive magnets and variable air gaps. In a different study [22], the high controllability of stiffness in the Dual-Segment Soft Robot was demonstrated, enabling sufficient stiffness for physical manipulation. In addition to the aforementioned studies, other research [23] focused on cooperative multi-agent reinforcement learning to simultaneously manage position and stiffness, aiming to reduce vibration in high-speed pick-and-place activities. Furthermore, investigations [24] have delved into the utilization of learning control methodologies in rigid VSG setups. Additionally, the pivotal role of position control in facilitating a refined grasp across different stiffness levels was emphasized in study [25]. The result showed big difference in stiff mode and rigid mode by using a fixed PID controller. Moreover, the 1-DOF VSG demonstrated in study [20] was capable of grasping fragile objects such as an egg and a wine glass, as well as relatively heavy objects, without the need for any soft cover or force/torque sensor. The aforementioned studies collectively illuminate the intricate challenges and notable achievements in the realm of VSG control. The capacity to adeptly modulate stiffness in response

to varying requirements is crucial, underscoring the enhanced functionality and applicability of VSGs in a diverse array of robotic tasks.

In our study, we developed a unique VSG that demands precise position and force control across a wide range of stiffness variations. While reinforcement learning is apt for soft actuators, it requires a sufficient number of samples for optimizing control, as shown in studies [23-24]. The other controllers are for specific designs, like the magnetic stiffness change in [14]. The PID controller [25] was used but not adaptable for variable stiffness. Achieving optimal performance across different stiffness modes remains challenging. Based on these, our project finds a better fit with robust control [26] due to its rapid adaptability to varying situations. To minimize the noise during the transition between force and position control in grasping, our research employs active disturbance rejection control (ADRC) [27,28], utilizing an extended state observer (ESO) for disturbance estimation. Our primary objective is to swiftly counteract discontinuous disturbances, whether from backlash nonlinearity or external factors. Additionally, we explore deterministic robust control (DRC) [29,30], noted for its high robustness and ability to handle stiffness changes. The comparative effectiveness of these two control systems against a standard PID controller is a key aspect of our research, focusing on their performance in managing uncertain parameters and disturbances. Although in the research stiffness range is large, robustness is the most significant parameter which cause DRC has a better performance than other two controllers. The primary contribution of this paper lies in demonstrating the dynamic behavior of the VSG and conducting a comparative analysis of various control systems on this dynamic model for stiffness varying grasping.

II. Design of the Proposed Gripper

A. Principle of Stiffness Variation

A continuous variable stiffness mechanism is presented in Fig. 1, consisting of a laterally hollow parallel guide beam and a solid rectangular block with the height and thickness consistent with cavity section. Based on the principle of changing the length of the parallel beam involved in the system, when the other parameters of the beam remain constant, the stiffness of the beam can be adjusted by inserting the long block from one end of the beam. In essence, this parallel beam can be considered as a pair of parallel leaf springs. As the length of the solid block inserted into the cavity increases, the lengths of the leaf springs in the system decrease, resulting in an increase in the stiffness of the beam. When the solid block is fully inserted, the entire parallel beam structure can be viewed as a solid cantilever beam with maximum stiffness. Inversely, by gradually retracting the solid block from the cavity, the length of the leaf springs involved in the system increases, leading to its stiffness decrease. When the solid block is completely removed from the cavity, the beam reaches the minimum stiffness.

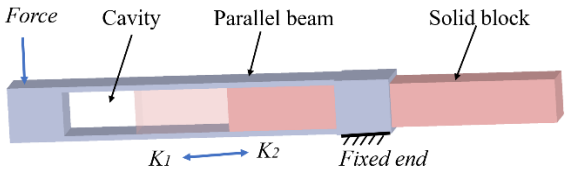

Figure 1. The principle of continuous stiffness change.

B. Mechanical Design

Utilizing the aforementioned principle as a basis, a VSG was devised, comprising a base, driving mechanism, and variable stiffness mechanism, as depicted in Fig. 2. The primary function of the VSG base is to accommodate diverse components, featuring threaded holes atop that facilitate connection to robotic arms via a connector. Positioned at the front of the base are two horizontal slides and one vertical slide, collectively forming the T-tracks along with six attached cover plates. These T-tracks enable sliders to undergo translational motion within their confines. In addition, the shell of the VSG is connected to the base through six brackets, which are not shown in the figure. The base of the VSG is primarily used to mount various components. The top of the base has threaded holes to connect with various types of robotic arms through connectors. On the front of the base, there are two lateral slides and one longitudinal slide. These slides, along with six cover plates fixed above them, collectively form five T-tracks, providing one degree of freedom for each slider to move. Additionally, a shell is connected to the VSG's base through six brackets to protect the whole gripper, which is not shown in the figure.

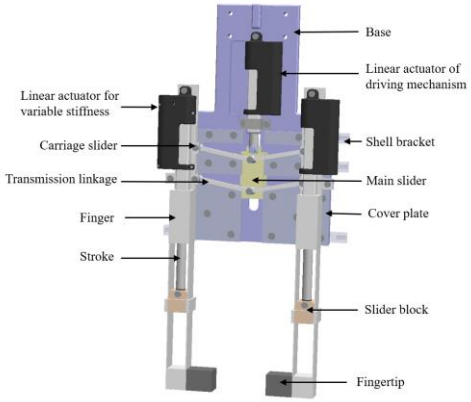

Figure 2. CAD model of the VSG.

The VSG features a sophisticated driving mechanism designed for parallel opening and closing of its two fingers, facilitating precise grasping and placement tasks. Utilizing two carriage blocks on T-tracks for lateral movement and connected via transmission linkages to a linear actuator, this setup enables smooth finger operation with a 50 mm stroke and 200N back drive force. For stiffness modulation, each finger incorporates a dedicated linear actuator (P16-100-22-12-P) with a 100 mm stroke, allowing rapid adjustment to the finger's rigidity by altering the segment of the parallel guide beam that the slider block traverses, achieving variable stiffness in just 2.2 seconds. The design emphasizes precision,

modularity with interchangeable fingertips, and the ability to adapt to various tasks through independently adjustable finger stiffness. Despite a limitation in the maximum opening between fingers, this is mitigated by customizable fingertip designs, such as arc-shaped ones with non-slip pads, enhancing grip stability and versatility of the VSG.

III. Analysis of the DVSA Dynamics for Force Control

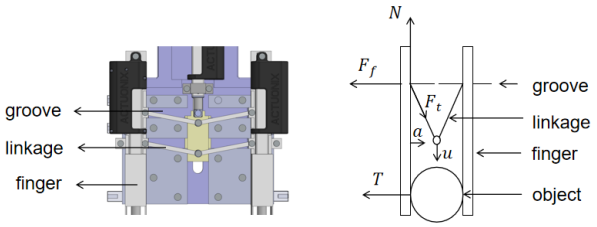

Figure 3. Mechanical diagram of a VSG.

The diagram presented in Fig. 3 is a mechanical representation of the VSG, illustrating the forces acting on a single finger. The input mechanism, upon activation, will exert a force on one side of the linkage system. This action will, in turn, cause the opposite side of the linkage to activate the fingers, compelling them to converge towards each other. The fingers will continue to move inward until they contact the object. Upon contact, they will apply sufficient pressure to securely grasp and lift the object. Force N represents the normal force exerted by the groove on the linkage, providing support against the linkage's movement. The input u denotes the output of the linear actuator, which is responsible for the motion of the linkage. This, in turn, applies a tensile force F_t, which is the pull exerted by the linkage on the finger. The frictional force F_f is the resistance encountered by the finger from the groove as the finger moves, opposing the direction of motion. The force T indicates the thrust force applied by an object onto the finger, typically resulting from the object being gripped or manipulated by the VSG. Lastly, the letter a symbolizes the acceleration of the finger as it interacts with the environment, influenced by the net forces acting upon it, including the tension, friction, thrust, and normal forces as described. From this, we can ascertain the dynamic equilibrium of the finger in the horizontal plane.

$$ma = \tan\theta \cdot u - F_f - F_t + d \tag{1}$$

(1) represents the dynamic model of the finger mechanism, the acceleration a of the finger is a resultant of the net force applied to it. The angle θ denotes the angle between the linkage and the finger, which influences the tangential component of the force generated by the actuator. The term d encapsulates the disturbances within the system, encompassing any external or unmodeled forces that might affect the finger's motion.

$$ma = \sqrt{\frac{l^2 - {x_t}^2}{{x_t}^2}}.u - \frac{\mu}{2} \cdot u - kx + d \tag{2}$$

(2) represents the specific expression of the finger dynamic model. The variable l represents the length of the linkage. The variable x_t signifies the total displacement of the finger from the initial position before contact to the final position after contact with the object. On the other hand, x specifically refers to the displacement of the finger after contacting the object. The coefficient of friction μ characterizes the frictional resistance encountered by the finger during interaction with the object's surface. Lastly, the constant k represents the stiffness of the finger mechanism, a parameter that determines the resistance of the finger to deformation under force. This stiffness plays a crucial role in how the finger adapts to the shape and surface of the object it is manipulating. we define that $x_1 = x, x_2 = \dot{x}_1 = V$, the dynamics of the DVSA torque control is modeled as:

$$\begin{cases} x_1 = x_2 \\ x_2 = \sqrt{\frac{l^2 - {x_t}^2}{4m^2 \cdot {x_t}^2}}u - \frac{\mu}{2m} \cdot u - \frac{k}{m}x_1 + \frac{d}{m} \\ y = kx_1 \end{cases} \tag{3}$$

Assume that $p = \sqrt{\frac{l^2 - {x_t}^2}{4m^2 \cdot {x_t}^2}} - \frac{\mu}{2m}$, we can get,

$$\begin{cases} \dot{x}_1 = x_2 \\ \dot{x}_2 = p.u - \frac{k}{m}x_1 + \frac{d}{m} \\ y = kx_1 \end{cases} \tag{4}$$

IV. Force Controller Design with Robust Compensation

In this section, we discuss the design of a controller that integrates force control upon contact with an object and position control when there is no contact. For position control, a PID controller is utilized, leveraging the encoder of the linear actuator for precision. To mitigate the impact of external disturbances and accommodate the wide variation in stiffness, a combination of PID, Active Disturbance Rejection Control (ADRC), and Deterministic Robust Control (DRC) are employed for the force control aspect of the VSG. These control strategies are selected for their efficacy in managing the complex dynamics of the VSG during operation.

A. LADRC

The prominent feature of ADRC is to employ an Extended State Observer (ESO) to estimate unknown disturbances [31], [32]. An ADRC controller has been developed, as illustrated in Figure 4, comprising an Extended State Observer (ESO) which has shown extraordinary performance in estimating disturbances or uncertainties and a Proportional-Integral (PI) controller which is designed to effectively address tracking errors.

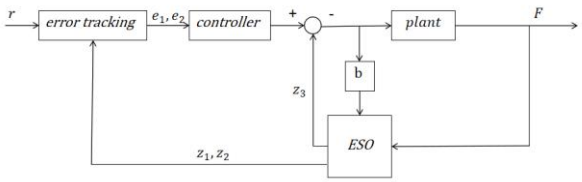

Figure 4. Active Disturbance rejective observer

To build an ESO, we assume $z_1 = \hat{x}_1, z_2 = \hat{x}_2, z_3 = \hat{x}_3$. β_1, β_2 and β_3 represent the observer gains. The equation of ESO can be written as:

$$\begin{cases} \dot{z}_1 = z_2 + \beta_1(y - \hat{y}) \\ \dot{z}_2 = z_3 + \beta_1 pu - \frac{k}{m}x_1 + \frac{d}{m} + \beta_2(y - \hat{y}) \\ \dot{z}_3 = \beta_3(y - \hat{y}) \end{cases} \tag{5}$$

Define that $z = [\, z_1, z_2, z_3]$, $u_c = [u, y]^T$ and $L\& = [\beta_1, \beta_2, \beta_3]^T$, We can get:

$$\begin{cases} z = [A - LC]z + [B, i]u_c \\ y_c = z \end{cases} \tag{6}$$

To make the error converge to zero, the eigenvalue should be less than zero. We can get $\lambda = [SI - CA - LC)] = s^3 + P_1S^2 + P_2S + P_3 = (StW_0)^3$, and the parameter can be found as $L = [3w_0, 3w_0^2, w_0^3]$. From Fig. 4, the controller is designed as a PD controller where β_{01} and β_{02} are the gains of the controller:

$$\begin{cases} e = v - \hat{x}_1 \\ u_0 = \beta_{01}e - \beta_{02}\hat{x}_2 \\ u = (u_0 - \hat{x}_3)/b \end{cases} \tag{7}$$

B. Determined Robust Controller Design.

A DRC is developed as in Fig. 5 based on slide mode control which is able to reduce the tracking error.

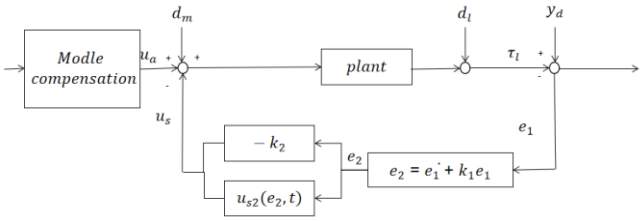

Figure 5. Deterministic Robust Control

Define $\theta_1 = \frac{1}{p}, \theta_2 = \frac{k}{mp}$, $\theta_3 = \frac{d}{mp}$, and the dynamic model can be written as:

$$\begin{cases} \dot{x_1} = x_2 \\ \theta_1\dot{x_2} = u - \theta_2 x_2 + \theta_3 \\ y = kx_1 \end{cases} \tag{8}$$

The tracking error can be defined as $e_1 = F - y_d$, and $e_2 = \dot{e_1} + k_1e_1 = e_2 - e_{2d}$. In this previous equation it can be found that the e_2 will be small or converge to zero when k_1 is a positive feedback gain. From $G_z(s) = \frac{e_1(s)}{e_2(s)} = \frac{1}{s+k_1}$, it can be known that e_1 will also be close to zero.

$$\begin{aligned} \theta \in \Omega_\theta \triangleq \{\theta: \quad \theta_{min} < \theta < \theta_{max}\ \} \\ \Delta \in \Omega_\triangleq \{\Delta: \quad |\ \Delta(x,t)\ | \leq \delta(x,t)\ \} \end{aligned} \tag{9}$$

As the uncertain parameters, we can get the minimum value $\theta_{min} = [\theta_{0\min}, \theta_{1\min}, \theta_{2\min}, \theta_{3\min}]^T$ and maximum value $\theta_{min} = [\theta_{0\max}, \theta_{1\max}, \theta_{2\max}, \theta_{3\max}]^T$, $\delta(x,t)$ is the known bound of the disturbance. Due to a certain bound (9) of the parameter and disturbance, the control input can be written as:

$$u = u_a + u_s \tag{10}$$

And from

$$\theta_0\dot{e}_2 = u + \boldsymbol{\psi}^T\boldsymbol{\theta} + \tilde{\Delta} \tag{11}$$

u_a can be defined as:

$$u_a = -\boldsymbol{\psi}^T\hat{\boldsymbol{\theta}} \tag{12}$$

$\theta = [\theta_0, \theta_1, \theta_2, \theta_3]^T$, and the regression which depends on the actual states e_1, e_2 can be written as $\psi = [-\dot{e}_{2\mathrm{d}}, -\dot{x}_2, -\dot{x}_1, 1]^T$, u_s is a robust control term as in Fig. 5 having the following forms:

$$u_s = u_{s1} + u_{s2} \tag{13}$$

$$u_{s1} = -k_2e_2 \tag{14}$$

u_{s1} is feedback to stabilize the nominal system and $k_2 > 0$ is a positive gain.

After defining each value of u_a from (12) and in u_s from (13) and (14), we can have (15) from subtract u_a and u_s from (11):

$$\dot{e_2} + k_2e_2 = u_{s2} - [\varphi(x)^T\tilde{\theta}_o - \Delta(x,t)] \tag{15}$$

The $\tilde{\boldsymbol{\theta}}_o$ is defined as $\tilde{\boldsymbol{\theta}}_o = \hat{\boldsymbol{\theta}}_o - \boldsymbol{\theta}$. The left side of Eq. (15) represents the stable nominal closed loop dynamics. The terms inside the brackets in Eq. (15) represent the effects of all model uncertainties. Though these terms are unknown, u_{s2} are bounded above with some known functions $h(x,t)$:

$$|\ \varphi(x)^T\tilde{\theta}_o - \Delta(x,t)\ | \leq h(x,t) \tag{16}$$

$$h(x,t) = \|\ \theta_{\max} - \theta_{\min}\ \|\| \psi \| + \delta_\Delta \tag{17}$$

With the SMC law, all signals in the system (5) are bounded and the output tracking error e_2 exponentially converges to zero. u_{s2} is a nonlinear robust performance feedback term to improve the robust performance and decrease the influence of parameter uncertainties. Therefore, as in DRC, if robust feedback u_{s2} can be synthesized so that the following conditions should be satisfied:

$$\begin{aligned} i. \quad & e_2(u_{s2} - \psi^T\tilde{\theta} + \tilde{\Delta}) \leq \varepsilon \\ ii. \quad & u_{s2}e_2 \leq 0 \end{aligned} \tag{18}$$

ε is a designed parameter that can be arbitrarily small. u_{s2} can be written as smooth example to satisfy $i.$ and $ii.$ which can be designed as:

$$u_{s2} - \frac{1}{4\varepsilon}h(x,t)^2z \tag{19}$$

V. Simulation

A conclusion section is not required. Although a conclusion may review the main points of the paper, do not replicate the abstract as the conclusion. A conclusion might elaborate on the importance of the work or suggest applications and extensions.

In this section, we apply the PID, ADRC, and DRC control strategies to the force control aspect of the VSG system. Two distinct performance simulations are conducted.

The first simulation is designed to demonstrate the step response of each method under varying levels of stiffness. This will provide insights into how each control strategy adapts to changes in the stiffness of the VSG. The second simulation closely mimics a real-world scenario involving the VSG. It encompasses the entire process of initially contacting an object, gripping it with low stiffness, and subsequently re-gripping with an increased stiffness. This simulation aims to evaluate the practical effectiveness and adaptability of the control methods in dynamic, real-life applications of the VSG. Table 1. are the parameters being used in the simulation.

Parameter	Value	Units
Range of stiffness variation (theoretically)	1~40.7	N/mm
Maximum design deflection (min. stiffness)	30	mm
Stiffness variation time from min. stiffness to max. (no load)	2.1	s
Maximum opening	106	mm
Effective length of the parallel beam	0 ~ 100	mm
Thickness of the parallel beam	1	mm
Gripper Dimension (L×W×H)	183×68×368	mm
Weight	728	g

TABLE I. MAIN SPECIFICATIONS OF THE VSG.

A. *Step Response*

The step response setup involves applying a sudden change in force from zero to 20N on a system and observing how the system responds to this change. The total duration of the step response setup is typically 1 second, during which time the system's response is recorded. For this setup, three different stiffness levels are to be tested, including 10 N/mm, 25N/mm and 40 N/mm. Each level represents a different level of resistance to the applied force and can be adjusted by changing the properties of the system. To simulate the response of the system to the applied force, the three different controllers are used including PID, ADRC and DRC.

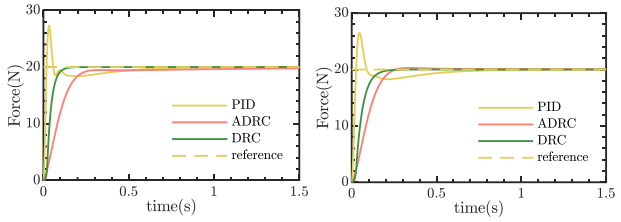

(a). k=10 N/mm (b). k=25 N/mm

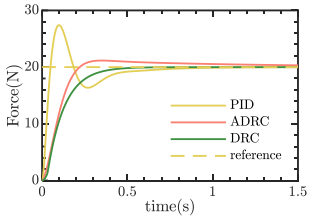

(c). k=40 N/mm

Figure 6. Step response for 3 controllers at different stiffness.

As depicted in Fig. 5, a comparative analysis of the step response characteristics of PID, ADRC, and DRC controllers is presented. Panels (a), (b), and (c) in the figure correspond to different stiffness levels of the finger, set at 10 N/mm, 25 N/mm, and 40 N/mm, respectively. It is evident from the data that the PID controller exhibits the longest settling time, with all three instances exceeding 0.5 seconds, whereas the ADRC shows a settling time over 0.5 seconds in only one case. Additionally, the PID controller which is tuned on 20N/mm demonstrates nearly 30% overshoot in this simulation, indicating a significant deviation beyond the desired response level. In contrast, the DRC controller delivers the fastest response among the three, consistently achieving settling times of less than 0.5 seconds across different stiffness levels. The most notable advantage of the DRC controller is its ability to completely eliminate overshoot in the system, ensuring a more precise and controlled response. This characteristic is particularly beneficial in applications where overshoot can lead to undesirable outcomes or system instability.

B. *Application scenarios*

This segment of the study simulates the operation of the VSG in grasping an object with unknown dimensions and characteristics. The entire simulation is divided into three distinct phases. The initial phase involves the VSG approaching the object with a lower stiffness setting, a process controlled using the encoder of the linear actuator. This ensures a gentle initial contact with the object, accommodating for its unknown properties. The second phase commences once the object has been contacted. In this stage, the VSG attempts to clamp onto the object. The final phase encompasses the release of the object, followed by a brief period of just touching it, and then re-gripping it with increased stiffness. This sequence allows for a more secure grasp on the object, especially important if the object needs to be manipulated or moved. The transition to higher stiffness is crucial for ensuring a firm and stable grip, particularly for objects that require a more robust handling approach. Therefore, in our simulation design, the initial phase is set with a speed of 2mm/s over a duration of 2 second. This gradual approach ensures a controlled and gentle contact with the object. For the second and third phases, the target clamping force is established at 20N. In these phases, the stiffness settings are varied, with the second phase using a stiffness of 25N/mm and the third phase employing a higher stiffness of 40N/mm. This adjustment in stiffness levels is critical for achieving the necessary balance between a secure grip and careful handling of the object.

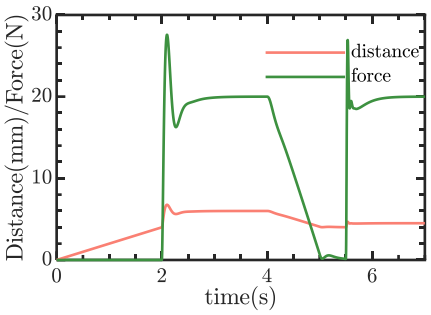

(a). PID

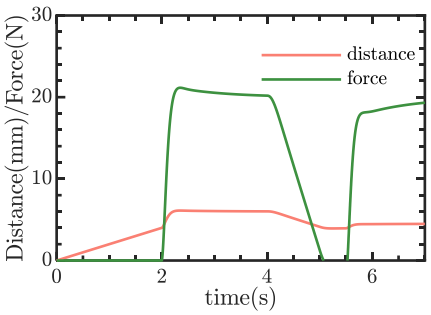

(b). ADRC

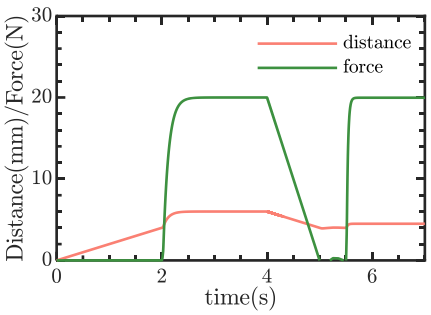

(c). DRC

Figure 7. Application scenarios

Fig. 7 presents the outcomes of position and force control simulations for the VSG system, particularly focusing on the transition from low to high stiffness modes under different force levels. In panel (a), the performance of the PID controller is analyzed. It is observed to have significant steady-state error and overshooting, which underscores its inadequate response to changes in stiffness. The ADRC, while exhibiting considerably less overshooting compared to the PID, still presents a noticeable steady-state error. In stark contrast, the DRC controllers demonstrate superior performance. Notably, the DRC controller achieves a remarkable balance with no overshoot and minimal steady-state error. These findings highlight the superior capability of the proposed control strategies, especially the DRC, in efficiently managing the stiffness transitions and force control challenges inherent to the VSG system.

VI. Conclusion

This paper introduces a novel concept and design for a VSG, complete with its dynamic modeling. Building upon this foundation, we developed and evaluated two control schemes in comparison with the traditional PID controller. These schemes are tailored for the combination of position and torque control, incorporating considerations for uncertainties in potential VSG application scenarios. In summary, while PID controllers are user-friendly, they fall short in dynamically adapting their gains to accommodate systems with variable stiffness and uncertain environments. ADRC demonstrates improved performance due to its capability to handle external disturbances. However, it struggles with significant changes in stiffness range. DRC controllers, on the other hand, offer superior control performance and robustness suitable for VSG systems, with DRC notably achieving greater stability and eliminating overshooting. Future research should focus on addressing uncertainties in system parameters and the operating environment. An exploration into more advanced controllers with adaptive capabilities is also recommended to further enhance the effectiveness of VSG systems.

Acknowledgment

This work is supported by the National Science Foundation (NSF) grant under CMMI-2131711

References

[1] X. Huang, R. Muthusamy, E. Hassan, Z. Niu, L. Seneviratne, D. Gan, and Y. Zweiri, “Neuromorphic Vision Based Contact-Level Classification in Robotic Grasping Applications,” Sensors 2020, Vol. 20, Page 4724 20(17), 4724 (2020).

[2] Zhang, B., Xie, Y., Zhou, J., Wang, K., & Zhang, Z. (2020). State-of-the-art robotic grippers, grasping and control strategies, as well as their applications in agricultural robots: A review. Computers and Electronics in Agriculture, 177, 105694. https://doi.org/10.1016/j.compag.2020.105694.

[3] Zhao, J., Gao, J., Zhao, F., & Liu, Y. (2017). A search-and-Rescue robot system for remotely sensing the underground coal mine environment. Sensors, 17(10), 2426. https://doi.org/10.3390/s17102426.

[4] Edsinger, A., & Kemp, C. C. (2007). Human-robot interaction for cooperative manipulation: Handing objects to one another. RO-MAN 2007 - The 16th IEEE International Symposium on Robot and Human Interactive Communication. https://doi.org/10.1109/roman.2007.4415256

[5] J. Y. Wang and C. C. Lan, “A constant-force compliant gripper for handling objects of various sizes,” J. Mech. Des. Trans. ASME 136(7) (2014).

[6] Q. Xu, “Design and Development of a Novel Compliant Gripper with Integrated Position and Grasping/Interaction Force Sensing,” IEEE Trans. Autom. Sci. Eng. 14(3), 1415 – 1428 (2017).

[7] A. N. Reddy, N. Maheshwari, D. K. Sahu, and G. K. Ananthasuresh, “Miniature compliant grippers with vision-based force sensing,” IEEE Trans. Robot. 26(5), 867 – 877 (2010).

[8] J. Gan, H. Xu, X. Zhang, and H. Ding, “Design of a compliant adjustable constant-force gripper based on circular beams,” Mech. Mach. Theory 173, 104843 (2022).

[9] J. Y. Wang and C. C. Lan, “A constant-force compliant gripper for handling objects of various sizes,” J. Mech. Des. Trans. ASME 136(7) (2014).

[10] Q. Xu, “Design and Development of a Novel Compliant Gripper with Integrated Position and Grasping/Interaction Force Sensing,” IEEE Trans. Autom. Sci. Eng. 14(3), 1415 – 1428 (2017).

[11] A. N. Reddy, N. Maheshwari, D. K. Sahu, and G. K. Ananthasuresh, “Miniature compliant grippers with vision-based force sensing,” IEEE Trans. Robot. 26(5), 867–877 (2010).
[12] L. Y. Lee, O. A. S. Malik, C. P. Tan, and S. G. Nurzaman, “Closed-Structure Compliant Gripper with Morphologically Optimized Multi-Material Fingertips for Aerial Grasping,” IEEE Robot. Autom. Lett. 6(2), 887–894 (2021).
[13] Zhu, M., Dai, J., & Feng, Y. (2023, July 21). Robust Grasping of a Variable Stiffness Soft Gripper in High-Speed Motion Based on Reinforcement Learning. Soft Robotics. https://doi.org/10.1089/soro.2022.0246
[14] X. Y. Guo, W. B. Li, Q. H. Gao, H. Yan, Y. Q. Fei, and W. M. Zhang, “Self-locking mechanism for variable stiffness rigid–soft gripper,” Smart Mater. Struct. 29(3), 035033 (2020).
[15] A. H. Memar and E. T. Esfahani, “A Robot Gripper with Variable Stiffness Actuation for Enhancing Collision Safety,” IEEE Trans. Ind. Electron. 67(8), 6607–6616 (2020).
[16] Y. Gao, X. Huang, I. S. Mann, and H. J. Su, “A Novel Variable Stiffness Compliant Robotic Gripper Based on Layer Jamming,” J. Mech. Robot. 12(5) (2020).
[17] K. B. Ham, J. Han, and Y. J. Park, “Soft Gripper using Variable Stiffness Mechanism and Its Application,” Int. J. Precis. Eng. Manuf. 2018 194 19(4), 487–494 (2018).
[18] M. Liu, L. Hao, W. Zhang, and Z. Zhao, “A novel design of shape-memory alloy-based soft robotic gripper with variable stiffness,” Int. J. Adv. Robot. Syst. 17(1) (2020).
[19] Y. Hao, T. Wang, X. Fang, K. Yang, L. Mao, J. Guan, and L. Wen, “A variable stiffness soft robotic gripper with low-melting-point alloy,” Chinese Control Conf. CCC, 6781–6786 (2017).
[20] B. S. Kim and J. B. Song, “Object grasping using a 1 DOF variable stiffness gripper actuated by a hybrid variable stiffness actuator,” Proc. - IEEE Int. Conf. Robot. Autom., 4620–4625 (2011).
[21] J. Fu, H. Lin, I. V. S. Prathyush, X. Huang, L. Zheng, and D. Gan, “A Novel Discrete Variable Stiffness Gripper Based on the Fin Ray Effect,” Lect. Notes Comput. Sci. (including Subser. Lect. Notes Artif. Intell. Lect. Notes Bioinformatics) 13457 LNAI, 791–802 (2022).
[22] Lai, J., Lu, B., & K. Chu, H. (2022, April). Variable-Stiffness Control of a Dual-Segment Soft Robot Using Depth Vision. IEEE/ASME Transactions on Mechatronics, 27(2), 1034–1045. https://doi.org/10.1109/tmech.2021.3078466
[23] Zhu, M., Dai, J., & Feng, Y. (2023, July 21). Robust Grasping of a Variable Stiffness Soft Gripper in High-Speed Motion Based on Reinforcement Learning. Soft Robotics. https://doi.org/10.1089/soro.2022.0246
[24] Kim, M., Niekum, S., & Deshpande, A.D. (2022). Scape: Learning Stiffness Control from Augmented Position Control Experiences. In Proceedings of the Conference on Robot Learning. Retrieved from proceedings.mlr.press.
[25] Li, X., Chen, W., Lin, W., & Low, K. H. (2018, July). A Variable Stiffness Robotic Gripper Based on Structure-Controlled Principle. IEEE Transactions on Automation Science and Engineering, 15(3), 1104–1113. https://doi.org/10.1109/tase.2017.2732729
[26] A. Calanca, L. Capisani, and P. Fiorini, “Robust force control of series elastic actuators,” Actuators, vol. 3, no. 3, pp. 182–204, 2014.
[27] Zuo, W., Song, G., & Chen, Z. (2022). Grasping force control of robotic gripper with high stiffness. IEEE/ASME Transactions on Mechatronics, 27(2), 1105-1116. https://doi.org/10.1109/tmech.2021.3081377
[28] Li, H., Cheng, L., Li, Z., & Xue, W. (2021). Active disturbance rejection control for a fluid-driven hand rehabilitation device. IEEE/ASME Transactions on Mechatronics, 26(2), 841-853. https://doi.org/10.1109/tmech.2020.3006364
[29] Utkin, V. I. (1977). Variable structure systems with sliding modes. IEEE Transactions on Automatic Control, 22(2), 212–222.
[30] Yao, B. (1996). Adaptive Robust Control of Nonlinear Systems with Application to Control of Mechanical
[31] J. Han, “From PID to active disturbance rejection control,” IEEE Trans. Ind. Electron., vol. 56, no. 3, pp. 900–906, Mar. 2009.
[32] Y. Huang and W. Xue, “Active disturbance rejection control: Methodology and theoretical analysis,” ISA Trans., vol. 53, no. 4, pp. 963–976, 2014.